CSIRO
AUSTRALIA

Improved AVHRR Data Navigation Using Automated Land Feature Recognition to Correct a Satellite Orbital Model

A. C. Dilley and C. C. Elsum

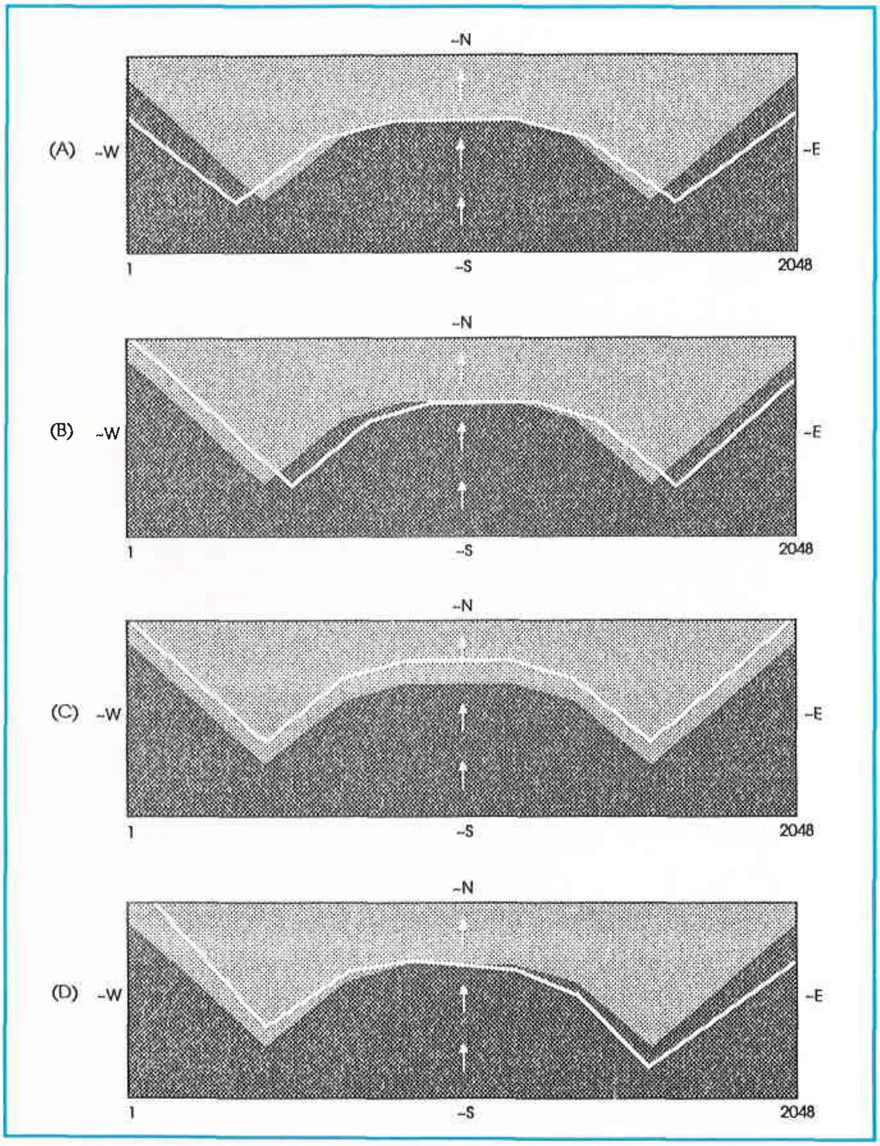

CSIRO DIVISION OF ATMOSPHERIC RESEARCH TECHNICAL PAPER NO.34

CSIRO
AUSTRALIA

Improved AVHRR Data Navigation Using Automated Land Feature Recognition to Correct a Satellite Orbital Model

A. C. Dilley and C. C. Elsum

CSIRO DIVISION OF ATMOSPHERIC RESEARCH TECHNICAL PAPER NO.34

National Library of Australia Cataloguing-in-Publication Entry

Dilley, A. C.
Improved AVHRR Data Navigation Using Automated Land Feature Recognition to Correct a Satellite Orbital Model.

Bibliography.
ISBN 0 643 05601 7.

1. Artificial satellites in remote sensing.
2. Artificial satellites — Orbits — Mathematical models.
3. Artificial satellites — Attitude control systems.
I. Elsum, C. C.
II. CSIRO, Division of Atmospheric Research.
III. Title. (Series: Division of Atmospheric Research technical paper; no.34).

621.3678

CSIRO Division of Atmospheric Research Technical Papers may be issued out of sequence.

Printed on recycled environmentally friendly paper

Improved AVHRR Data Navigation Using Automated Land Feature Recognition to Correct a Satellite Orbital Model

A. C. Dilley and C. C. Elsum
CSIRO Division of Atmospheric Research
Private bag 1 Mordialloc Victoria 3195
Australia

Abstract

An operational procedure for the automatic navigation of daytime image data from the Advanced Very High Resolution Radiometer (AVHRR) is described. The procedure achieves greater accuracy than methods which rely solely on models of satellite orbit and attitude. It applies a land feature recognition technique to determine the errors generated across an image using the Brouwer-Lyddane model of satellite orbit and assuming zero error in satellite attitude and radiometer alignment. It then uses a non-linear least-squares regression technique to determine corrections which need to be applied to the satellite position in order to minimize residual errors across the image. Corrections to the model-predicted satellite position and attitude in terms of satellite height, cross-track position, along-track position and yaw are derived as a linear function of image line number. Related coefficients are recorded in the header of each processed image data file whence they are accessed and used by image navigation algorithms to provide line-by-line corrections to model-predicted position and attitude.

Some of the corrections show a consistent bias — a cross-track correction for the NOAA-11 satellite and a cross-track and yaw correction for the NOAA-12 satellite — suggesting a mechanical misalignment of instruments and/or a permanent bias in the satellites' attitude control systems.

Under conditions where the number and distribution of identified land features is sufficient to allow full analysis (~60-70% of daytime overpasses using the current implementation), the method provides navigation to an accuracy of $\sim \pm 1$ pixel/line for pixels which lie within ± 800 pixels of the centre of the swath. Under operational conditions, this performance is only marginally reduced.

1 Introduction

Image data recorded by the Advanced Very High Resolution Radiometer (AVHRR) — a 5-band scanning radiometer carried by the Advanced TIROS-N (ATN) series of polar-orbiting meteorological satellites — have found wide application in numerous environmental monitoring and resource management tasks. Essential to many such applications is the means of accurately referencing an image element to a location on the ground. In other words, one requires an accurate transformation from image data co-ordinates to geographical co-ordinates. In some applications one needs to identify a geographic location in the image data and the reverse transformation is required. For obvious reasons, the process of applying these transformations is commonly known as image navigation. Once accurate navigation algorithms are established, the task of remapping image data to any required map projection is essentially trivial.

The mechanical characteristics of the AVHRR are well documented (e.g. Planet, 1988). Hence, if a satellite's position and attitude at the time of measurement of an image element are known accurately the ground location of that image element can be calculated with commensurate accuracy.

Position can be calculated using an orbital model. Such models extrapolate position as a function of time elapsed since a base time, known as the epoch, for which relevant ephemeris data have been calculated or determined. The accuracy of the position parameters so generated is thus a function of the accuracy of the ephemeris data, the model and one's clock. While errors can be minimised by regularly updating ephemeris data, most navigation methods which rely on orbital models alone produce results that are less than satisfactory for most applications. Using such methods, Brunel and Marsouin (1989) report an overall accuracy of ~ 3 km while Kloster (1989) reports a figure of ~ 10 km. The results obtained vary with the implementation and the way in which the various sources of error are treated. Emery *et al.* (1989) provide a comprehensive overview of methods which rely on orbital models; Krasnopolsky and Breaker (1994) review sources of error.

For the ATN series of satellites attitude is sensed and corrected by the Attitude Determination and Control System (ADACS). Roll and pitch are controlled using horizon sensors while yaw is controlled using sensors which sight on the sun once per orbit. The system is designed to maintain all attitude components (roll, pitch and yaw) within a ± 3.5 mrad specification (Schwalb, 1982). Operational experience has shown that roll and pitch are normally maintained to a much greater accuracy than their specification whereas yaw is less well maintained and can frequently exceed its specified maximum. Clift (private communication) reports evidence of a small slowly varying roll error, small periodic pitch transients and a yaw variation of up to 2.5 mrad during an orbit. Krasnopolsky and Breaker (1994) report roll and pitch being maintained to within $\sim 10\%$ of the specified maximum but yaw varying by up to double the specified maximum in periods as short as 10 minutes. A 7.0 mrad error in yaw translates to ~ 10 km error in navigation at the edge of an overpass swath.

More accurate specification of position and attitude can be achieved in a number of ways. For example, Clift *et al.* (unpublished) report development of a more accurate orbital model. But gains in this area cannot be fully realized in terms of improved image navigation until there is corresponding development of accurate models of satellite attitude variation, in particular yaw variation, or some other means are used to

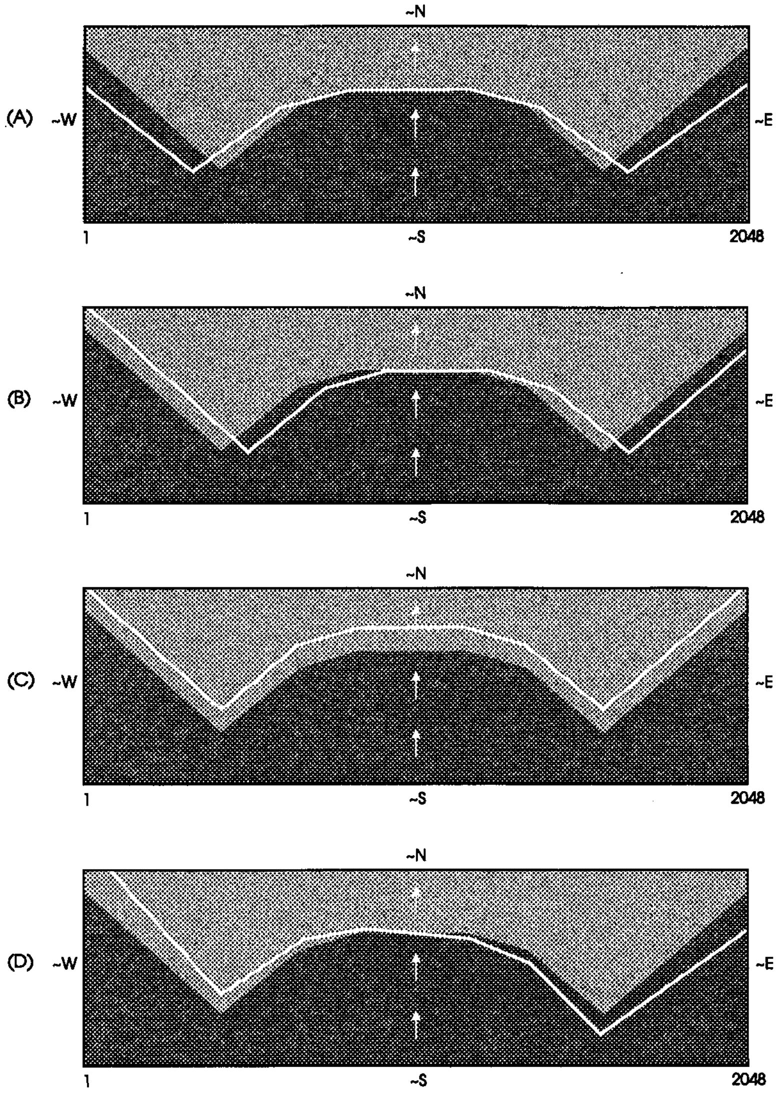

Figure 1: Diagrammatic representation of AVHRR imagery showing the effects on coastline mapping of incorrectly predicted satellite position and attitude. The white arrows show the satellite ground track of an ascending overpass. The white lines show where the coastline is calculated to lie in instances where: (A) predicted satellite height is too low; (B) predicted satellite cross-track position is too far West; (C) predicted satellite along-track position is too far South; (D) assumed satellite yaw is too far anti-clockwise.

accurately specify attitude.

The present report describes an empirical method of arriving at both position and attitude during daylight hours. It uses the satellite imagery itself to fine tune yaw and correct satellite position relative to a position predicted by the Brouwer-Lyddane orbital model (Brouwer 1959, Brouwer and Clemence 1961, Lyddane 1963, Capellari *et al.* 1976).

Various methods of using the satellite imagery to improve navigation accuracy have been reported. Emery *et al.* (1989) review methods in which the locations of features in the image are found manually and used to refine the mapping algorithm. Kloster (1989) reported significant improvement in accuracy with the location of just one feature in the image. Cracknell and Paithoonwattanakij (1989) adapted a method pioneered by Torlegård (1986) to fully automate the process of feature location and obtained further improvements in accuracy by using Landsat Multi-Spectral Scanner (MSS) data for feature identification. Eidenshink (1992) used 250 common features to perform automatic image-to-image registration. Bordes *et al.* (1992) report an adaptation of an automatic procedure developed by Jullien and Phulpin (1988) to locate coastal landmarks; it reduces overall error to 0.8 pixel and 1.0 line for 86% of overpasses analysed. However, Brunel and Marsouin (1992) found the method of Bordes *et al.* to produce an error which increases with increasing distance cross-track from nadir for NOAA-12 images. Robertson *et al.* (1992) report on a system which automatically locates features using sub-images derived from Landsat MSS data. Errors relative to locations provided by the underlying orbital model are then used to appropriately modify ephemeris data. The method is capable of sub-pixel accuracy within the view angle of $\pm 45^\circ$ with as few as 10 located features. Baldwin and Emery (1993) describe a method which requires as few as two features to be located in the image. Offsets to these locations from those based on an ephemeris-driven orbital model are used to compute 'effective' values of roll, pitch and yaw which remain constant for any given data set. The method is reported to yield an accuracy of 1 pixel.

The method described here is similar to the automated methods referenced above but distinguished from them notably by the technique used for land feature location within the image and the use made of image registration errors to compute corrections to predicted satellite position (height, cross-track and along-track position) and attitude (yaw) as a linear function of image line number.

2 Method

2.1 Underlying principles

Some appreciation of the approach employed here can be gained by reference to figure 1. Diagrams show the errors in image navigation resulting from various errors in predicted satellite position and assumed attitude. Errors in cross-track location of the fitted coastline of the type shown arise when the predicted satellite position is lower (A) and further West (B) than its true position. Similarly, errors in along-track location of the fitted coastline arise when the predicted satellite position is further South than its true position (C) and the assumed yaw is further anticlockwise than its true yaw (D).

Thus, in principle, the predicted height and cross-track position of the satellite could be adjusted to minimize errors in cross-track location of the fitted coastline while the predicted along-track position and assumed yaw could be adjusted to minimize errors in along-track location. The final position and yaw arrived at would approximate closely the true position and yaw of the satellite.

A similar procedure is used here. However, instead of coastlines, small subsets of previously recorded images are used to find the true position in the image of various geographical features. Known as chips, these subsets each have at their centre a uniquely defined geographic feature such as a cape or a confluence of two rivers, the geographic co-ordinates of which are known. The chip data are correlated with the image data at successive line and pixel offsets relative to an initial position given by application of the Brouwer-Lyddane orbital model and the assumption of zero error in attitude. Where the correlation peaks is the location in the image of a specific geographic feature, i.e. the 'true' location in the image of specific geographic co-ordinates. Using a library of chips, a table is built of corresponding image and geographic co-ordinates, otherwise known as ground control points (GCPs), of features spread throughout the image.

It is assumed that the differences between the true position parameters and those predicted by the orbital model vary slowly relative to the duration of a full overpass. Similarly yaw is assumed to vary only slowly. Hence position and yaw corrections are allowed to vary linearly with image line number. Thus satellite height, h, is descibed by the equation:

$$h = h_B + c_{0,h} + c_{1,h} l \tag{1}$$

where h_B is the height given by application of the Brouwer-Lyddane orbital model, $c_{0,h}$, $c_{1,h}$ are constants to be determined and l is the image line number. Similarly, cross-track position, x, along-track position, y, and yaw, ϕ, are described respectively by the equations:

$$x = x_B + c_{0,x} + c_{1,x} l \tag{2}$$

$$y = y_B + c_{0,y} + c_{1,y} l \tag{3}$$

$$\phi = c_{0,\phi} + c_{1,\phi} l \tag{4}$$

No adjustment is made for roll or pitch. Errors in image navigation due to perturbations in roll and pitch are almost indistinguishable from the effects of error in predicted cross-track and along-track position respectively and can be compensated for by corrections to these.

The values of the constants in equations 1 – 4 are determined using a non-linear least-squares algorithm. It produces values of constants in equations 1 and 2 for which residual errors in image cross-track location are a minimum and values of constants in equations 3 and 4 for which residual errors in image along-track location are a minimum.

2.2 AVHRR characteristics

The AVHRR optical system scans $\pm 55.4°$ from nadir in 2048 equal steps with a field of view of 1.3 mrad. The effects of this configuration for a satellite orbiting at a height of 850 km are shown in table 1. There is marked non-linearity between steps (which translate directly into pixels in the image) and corresponding ground distance across the scan. At nadir the ground increment between steps is 0.803 km and the field of view is 1.11 km. Both these parameters double in the first 750 steps from nadir and double again in the next 220 steps.

pixel number	x	Δx	FOV	$x/\Delta x$
1024	.4	0.80	1.11	0.5
1274	205.7	0.86	1.18	256.3
1524	442.8	1.07	1.48	551.6
1774	770.3	1.65	2.27	959.8
2024	1397.5	4.09	5.62	1741.2

x cross-track ground distance from nadir to centre of pixel (km)
Δx cross-track ground increment between pixels (km)
FOV field of view in terms of ground coverage (km)

Table 1: AVHRR cross-track characteristics for satellite at height of 850 km.

The ground increment between successive scans is 1.1 km. Thus, at nadir and for most of its swath, the AVHRR provides full coverage of the earth's surface with insignificant overlap. However, nearer the edge of the scan, pixels have overlapping fields of view, leading to lack of resolution of detail in these areas.

The AVHRR instrument is carried by satellites in approximately sun-synchronous near polar orbits with an inclination of $\sim 99°$. Thus, the scanline orientation relative to lines of latitude varies markedly depending on whether the satellite is travelling approximately North (ascending) or approximately South (descending).

2.3 Non-linear and linear pixels

The non-linearity between pixels and cross-track ground distance from nadir described above means that sub-images of the same location extracted from different overpasses are not directly comparable — each will be distorted variously according to the satellite position relative to the location at the time of data capture. Thus, in order to compare a chip with a corresponding area in an image, it is necessary to have both the chip and the area mapped to a common co-ordinate system.

For the present work the common cross-track unit is defined as the cross-track ground increment between pixels at nadir, i.e. Δx_{1024} km, for a satellite at a height of 850 km. It is referred to as a linear pixel because it is linear with respect to cross-track ground distance — 1 linear pixel = 0.803 km. The last column in table 1 gives the cross-track ground distance from nadir to pixel centre in units of linear pixels. Selecting the smallest ground increment normally encountered as the common cross-track unit ensures optimal use of available data in subsequent image correlation and feature collocation.

Conventionally an AVHRR image has an image co-ordinate system of pixel number and lines where pixel number ranges between 1 and 2048 and line number ranges between 1 and n where n is the last line recorded. This scheme can be extended to the concept of a linear pixel number. A standard or 'non-linear' pixel number is transformed to a linear pixel number using

$$lpn = INT\left(\frac{x_{nlpn}}{0.803} + 1999.5 \right) \qquad (5)$$

where lpn is the linear pixel number corresponding to the non-linear pixel number, $nlpn$ and x is the cross-track ground distance from nadir to centre of the non-linear pixel in km. Thus the linear co-ordinate system has linear pixel numbers 2000 and 2001 spanning the nadir point. It has the same line numbers as the non-linear co-ordinate system. Note that x_{nlpn} is a function of satellite height and hence the values obtained on applying the transformation from non-linear to linear pixel numbers vary from overpass to overpass and even within an overpass.

2.4 Sub-scenes of geographic features — chips

Chips are small sub-scenes of an image centred on a distinctive ground feature. The geographic location of the feature is known precisely and recorded in the chip header to an accuracy better than $\pm 0.005^\circ$ latitude/longitude (corresponding approximately to ± 0.5 line/pixel).

Areas of images selected for chip creation need to meet the following criteria:

- a clear view of a central feature is provided, i.e. the sub-area is not contaminated by cloud, sun-glint, dropouts, etc.;
- the feature has a unique shape within the sub-area which allows accurate alignment with a second image of the feature in both the cross-track and along-track directions;
- the area surrounding the feature includes extensive areas with permanent, contrasting signal levels;
- the sub-area is extracted from an area lying within the central 1000 pixels of the overpass image — this ensures adequate feature definition at the required scale, i.e. a single pixel;
- the resulting set of chips covers the area of interest as uniformly as possible.

Once an area is selected for chip creation the original image data in the area are remapped to a linear co-ordinate subset of size 65 linear pixels by 65 lines by 5 channels. This is a larger volume than is actually used in feature location but provides for possible future developments. The remapped data are written as an image file and the latitude and longitude of the feature at the central pixel are recorded in the image header. The chip file name and its latitude and longitude are recorded in a chip library register.

The differing orientations relative to the earth of images from ascending and descending overpasses means that a chip made from an ascending overpass is not directly comparable with image data from a descending overpass. Hence two sets of chips are required — one for ascending overpasses, the other for descending overpasses.

The present operational system uses 300 chips for ascending overpasses spanning continental Australia and Tasmania and 150 chips for descending overpasses spanning all states except Western Australia. Lack of suitably defined features in inland areas has forced uneven distribution with the bulk of chips concentrated in coastal areas.

2.5 Locating geographic features in an image

For every overpass to be processed, the chip register is read sequentially and the chip's location within the overpass calculated using a Brouwer-Lyddane orbital model and assuming zero error in satellite attitude and instrument alignment. (The calculations assume that attitude is maintained with respect to the local horizons of a non-spherical earth.) If this location lies within the central 1600 pixels of the overpass an area of the image centred on this location is extracted. The extracted data are remapped to a linear co-ordinate subset of size 117 linear pixels by 75 lines by 1 channel (AVHRR band 2) still centred on the *calculated* location in the image of the chip's central feature. This is a larger area than is actually used in feature location but, again, provides for possible future developments. Band 2 is used because it has been found to have greater signal variation and hence better feature definition than other AVHRR bands.

A splinter is formed from the chip. It is 33 linear pixels by 33 lines by 1 channel (band 2). An image scan area is defined — 85 linear pixels by 43 lines about the image subset centre. Data from an area 33 linear pixels by 33 lines centred on the top left hand corner of the scan area are linearly correlated with the splinter data and the linear correlation coefficient, r_0, calculated using

$$r_0 = \frac{s_{xy}}{s_x s_y} \tag{6}$$

where s_{xy} is the covariance between the splinter data, x, and the image data, y, and s_x and s_y are the standard deviations of the splinter and image data respectively.

Correlation is repeated with image data centred on the next pixel in the scan area and subsequently for all pixels in the scan area and hence an array of r_0 values is generated. If the maximum r_0 value in the array exceeds some critical value which, in the present implementation is set to 0.90, the feature is said to have been 'found'. The location of the feature relative to its calculated location is given by the offset of the co-ordinates of the maximum r_0 value relative to the central pixel in the image data.

The procedure outlined above yields *integer* offsets of the true location in the image from the calculated location in terms of linear pixels and lines. In practice, *real* offsets in these units are calculated by fitting a surface to points in the r_0 array in the vicinity of the maximum value and determining the real co-ordinates of the maximum of that surface.

A further variation on the above is introduced in order to reduce processing time. Under operational conditions, many ground features are obscured by cloud so that relatively few correlations of splinter and image data yield r_0 values approaching the critical value. Hence, in the first instance, the correlation is performed on a subset of the available data, a 3 by 3 decimation. If this produces a value of $r_0 > 0.80$ then a correlation is performed on the full data set.

2.6 A ground truth table of geographic feature locations

Once a feature is 'found', details, including geographic location, calculated location in the image and offsets to its true location in the image, are registered in a ground truth table of geographic feature locations. Each entry in the table corresponds to an image-located feature. The table provides the GCP data which form the basis of all subsequent analysis. It also provides auxilliary data which are used to construct a comprehensive report.

2.7 Non-linear least-squares analysis

Values of the constants in equations 1 – 4 are determined using a non-linear least-squares algorithm formulated by Wright and Holt (1985). An external function is supplied to the algorithm which calculates for each GCP the residual error in image cross-track location. The function is constrained by equations 1 and 2 with constants initialized to zero. A second external function is supplied which calculates the Jacobian of the first function. The least-squares algorithm then yields values for the four constants $c_{0,h}$, $c_{1,h}$, $c_{0,x}$, $c_{1,x}$ for which residual errors in image cross-track location are a minimum — and hence linear corrections in satellite height and cross-track position. The procedure is repeated with an external function which calculates for each GCP the residual error in image along-track location. This function is constrained by equations 3 and 4. In this case the least-squares algorithm yields values for the four constants $c_{0,y}$, $c_{1,y}$, $c_{0,\phi}$, $c_{1,\phi}$ for which residual errors in image along-track location are a minimum — and hence linear corrections in satellite along-track position and yaw.

2.8 Results of analysis - storage and subsequent use

At the conclusion of the non-linear least-squares analysis, the eight derived constants are stored in the image header. In addition, a flag in the image header is set to indicate that satellite position correction parameters are available.

Whenever it is called, the primary low-level navigation routine reads the correction flag and, if it is set, applies linear corrections to the satellite position parameters generated by the Brouwer-Lyddane model. The routine uses equations 1 – 4 and the stored correction constants.

2.9 Distribution of located geographic features — constraints

Ideally, GCPs would be distributed reasonably uniformly across the image to be analysed. In practice such distributions are rarely encountered. One compounding factor is that chips are centred mostly on features in coastal areas. Another is that cloud often masks extensive contiguous areas.

The present method makes only rudimentary checks on distribution of GCPs and imposes simple rules to deal with cases where the checks show the distribution to be inadequate. The ground truth table is scanned to check that a critical number of cross-track pixels separates the two GCPs with lowest pixel number from the two GCPs with highest pixel number. It is then scanned similarly to check that a critical number of along-track lines separates the two GCPs with lowest line number from the two GCPs with highest line number. These critical values are operator selectable but have default values of 500 for cross-track pixels and 1000 for along-track lines. For images covering the whole of the Australian continent, default values are invariably accepted and were used to obtain the results shown and discussed below.

The procedures followed in cases where the distribution of points is found to be inadequate are summarised in table 2. Where the cross-track distribution is inadequate and the along-track adequate, there is considered to be insufficient data to resolve corrections to height and yaw and no corrections to these parameters are attempted. For the converse case of adequate cross-track distribution and inadequate along-track distribution, there is considered to be insufficient data to resolve along-track variation in all four parameters and no along-track variation is allowed. In the case where the distribution of GCPs is inadequate in both directions, the only correction that is allowed is an offset in satellite cross-track and along-track position which is invariant with along-track position.

cross-track distribution	*along-track distribution* adequate	inadequate
adequate	all c values calculated	$c_{1,h} = c_{1,x} = 0$ $c_{1,y} = c_{1,\phi} = 0$
inadequate	$c_{0,h} = c_{1,h} = 0$ $c_{0,\phi} = c_{1,\phi} = 0$	$c_{0,h} = c_{1,h} = c_{1,x} = 0$ $c_{1,y} = c_{0,\phi} = c_{1,\phi} = 0$

Table 2: Constraints on corrections for various distributions of GCPs

Apart from distribution, the actual number of GCPs impacts on analysis procedures to be followed. If the number falls below some critical number, which in the present implementation is set at 11, then there is considered to be insufficient data to resolve all the c values and analysis is restricted to determining $c_{0,x}$ and $c_{0,y}$ with all other c values set to zero - i.e. as per the case where the distribution of GCPs is inadequate in both directions.

3 Implementation in Software

The method described above is implemented in Fortran code using the methodologies and lower-level routines of a commercial image processing package.

Three independent, stand-alone utilities have been written: CHIPS, REGERR and SATLOC. The function and operation of these are described below.

3.1 CHIPS

The CHIPS utility guides the operator through the selection of areas suitable for chip creation, the creation of the chip itself and its registration in the chip register.

The operator works with a full resolution subset of a displayed image and selects a feature on which the chip can be based bearing in mind the criteria for selection outlined above. The image is zoomed by a factor of 8 and the feature accurately located using cursor and mouse. The operator is then prompted for the latitude and longitude of the feature. The rest of the processing (chip creation and registration) is performed automatically. The whole process is simply performed and takes only a few tens of seconds to complete.

The presence of 'dropouts' (i.e. isolated pixels with values very different from the values of surrounding pixels) reduces the effectiveness of a chip. Therefore, in making a chip, the raw data of the source image are passed through a filter which replaces 'dropout' pixels with the mean value of pixels surrounding them.

3.2 REGERR

The REGERR utility is designed to graphically illustrate to the operator where chips are located in the image and the size of the registration error, i.e. the difference between the calculated location of a feature and the true location of that feature in the image.

The operator works with either a decimated or full resolution subset of a displayed image. In the case where the image has had correction coefficients calculated and stored, the operator selects whether the uncorrected or corrected orbital model is to be used in navigation calculations. REGERR overwrites on the display small crosses which mark the locations of the centre-points of chips as given by either the uncorrected or corrected orbital model. The operator selects a chip using cursor and mouse and the utility then displays a 'zoomed' image of the selected chip and alongside it the 'zoomed', linearized image of the area normally used in the correlation process (i.e. 117 linear pixels by 75 lines). Both images have a pair of grid lines drawn over them intersecting at the centre-point. Thus the operator is presented with images which illustrate the current registration error in graphic detail. In the case where the operator has chosen to use the *uncorrected* orbital model (or where no correction coefficients are available) the images reflect the situation as it would exist in the main processing algorithm immediately prior to correlation between chip and image. In the case where the operator has chosen to use the *corrected* orbital model the images reflect the situation as it would exist at the conclusion of the non-linear least-squares analysis. An option allows the operator to list the array of r_0 values.

3.3 SATLOC

The SATLOC utility encodes the satellite position and attitude correction algorithm described above. It is written for either interactive or batch processing and requires the following minimal input: the filename of the image data (normally a full overpass); the filename of the processing report; the critical distance between pixels for adequate cross-track spread of GCPs; the critical distance between lines for adequate along-track spread of GCPs; whether to perform analysis on the whole image or a subset — if the latter, the dimensions of the subset.

It writes calculated correction coefficients to the image header and writes a report to the designated file. The detail in the report is governed by a 'user print message level' parameter — at its most comprehensive the report lists the correlation coefficient and offsets for each pixel, provides statistics on pre- and post-analysis registration errors and identifies GCPs with greatest residual errors.

Installed on a SUN IPX workstation, SATLOC completes analysis of a full overpass in 4 – 5 minutes.

4 Performance

Following some early trials, the SATLOC utility was scheduled in January 1992 to automatically process the image data of every new NOAA daytime overpass acquired via the satellite data reception facility operated by the CSIRO Division of Atmospheric Research (DAR). The batch process uses default values for critical distances defining adequate spread of identified GCPs and analyses the whole of the received image. A slightly modified version of SATLOC has been used operationally for almost 2 years in the VEGETATION WATCH project run under the auspices of DOLA[1] and CSIRO at the Leeuwin Centre for Earth Sensing Technologies at Floreat, Western Australia.

The value of the approach described here was assessed using the performance statistics listed in SATLOC's report files and the improvements in accuracy of navigation utilities when those utilities made use of the satellite position correction parameters generated by SATLOC. The conclusion reached after using the system operationally since its implementation to the present at DAR and for the previous two years in Western Australia is that the approach dramatically improves navigation accuracy over land in all but an exceedingly small number of received daytime overpasses. Even when only a small number of GCPs can be identified, the approach significantly reduces the mean error if not the variance of the error.

Here we attempt to quantify the value of the approach by examining the performance statistics listed in SATLOC report files. We consider performance under two headings — first, assessment of the methodology where identified GCPs are sufficient in number and distribution to allow retrieval of a full set of correction parameters and, second, performance as an operational procedure where identified GCPs are not necessarily sufficient in number and distribution to allow retrieval of a full set of correction parameters.

4.1 Assessment of the methodology

Reported performance statistics for 35 daytime NOAA-11 and 35 daytime NOAA-12 overpasses are listed in tables 3 and 4 respectively. Overpasses for both tables were selected to provide examples which varied in time and season within the constraint that identified GCPs for each overpass were sufficient in number and distribution to allow retrieval of a full set of correction parameters.

The tables show mean values of pre-analysis cross-track errors which are relatively invariant and always positive for NOAA-11 and negative for NOAA-12 overpasses. Mean values of pre-analysis along-track errors are much more variable — which is to be expected as along-track errors are due in large part to variations in system clock time. The consistency of cross-track errors leads one to expect a consistent bias in the satellite cross-track position correction for both satellites.

Neither satellite position correction parameters nor actual correction values are included in tables 3 and 4. However a summary of corrections corresponding to the data listed in these tables is shown in graphical form in fig. 2. Along-track corrections are not included in the figure for the reason outlined above. Other corrections are shown as a function of line number with a straight line drawn through the mean values at selected line numbers and error bars indicating ± 1 standard deviation about the mean. The variance in the NOAA-11 plots is least in the $2000 - 5000$ line number range whereas the variance in the NOAA-12 plots is least in the $1 - 3000$ line number range — behaviour consistent with the fact that these are regions where the NOAA-11 and NOAA-12 satellites overfly the Australian continent in the ascending and descending nodes of their of respective orbits. Small errors in the slope of the linear correction function derived using land features sometimes produce relatively large absolute correction errors when the function is extrapolated to ocean areas.

[1] Department of Land Administration, Government of Western Australia.

orbit	date	pts	cross-track					along-track				
			pre-analysis		post-analysis			pre-analysis		post-analysis		
			$\overline{xt}$	σ_{xt}	$\overline{xt}$	σ_{xt}	$xt\%$	$\overline{at}$	σ_{at}	$\overline{at}$	σ_{at}	$at\%$
15528	30/09/91	51	2.0	1.2	0.1	1.1	84	1.9	0.8	0.0	0.8	94
15726	14/10/91	73	2.9	2.5	0.1	1.4	77	-9.0	1.2	-0.2	1.0	89
17081	18/01/92	29	1.6	1.5	0.1	1.3	72	-8.8	1.7	-0.1	0.9	93
17886	15/03/92	14	4.0	3.3	0.0	1.3	86	1.3	2.3	-0.2	1.6	57
17900	16/03/92	21	2.7	1.5	-0.1	1.2	81	10.2	1.3	0.0	1.1	81
18027	25/03/92	39	1.9	1.6	0.1	1.3	69	4.2	1.1	-0.1	1.0	87
19100	09/06/92	34	0.9	1.0	-0.1	0.9	91	-0.9	1.0	-0.1	1.0	91
19199	16/06/92	40	1.5	1.6	-0.1	1.3	78	5.4	1.2	0.1	1.2	83
19213	17/06/92	25	2.1	0.9	-0.0	0.9	88	6.3	1.6	0.0	1.0	88
19227	18/06/92	33	1.6	1.0	0.0	1.0	82	10.7	0.8	-0.0	0.8	94
19665	19/07/92	50	3.0	1.9	0.0	1.2	82	1.8	1.5	0.0	1.0	84
19679	20/07/92	45	2.7	1.2	-0.0	1.1	78	-0.4	1.3	-0.0	1.0	93
19693	21/07/92	34	2.1	1.6	0.0	0.9	88	-1.9	0.8	0.0	0.7	94
20272	31/08/92	33	2.3	1.0	0.0	0.9	88	2.0	1.2	-0.0	1.0	91
20371	07/09/92	38	4.1	1.3	0.0	1.1	79	-0.9	1.3	-0.0	1.0	87
20385	08/09/92	29	2.8	1.1	0.0	0.9	90	3.3	1.8	0.0	0.9	93
20413	10/09/92	14	3.0	1.5	0.0	0.6	100	2.0	0.8	0.0	0.7	100
20498	16/09/92	47	2.5	1.3	-0.0	1.0	89	0.8	1.6	-0.0	0.8	96
20823	09/10/92	43	4.6	2.5	0.0	1.2	78	6.5	1.6	0.0	1.0	86
20837	10/10/92	35	3.1	1.5	0.0	1.0	91	7.9	1.6	-0.0	1.0	89
20978	20/10/92	29	2.2	1.2	-0.0	1.1	83	-11.5	0.8	0.0	0.7	93
21063	26/10/92	43	4.1	2.6	0.0	1.1	77	-5.8	1.4	-0.0	0.8	93
21077	27/10/92	31	2.8	1.5	0.0	1.0	87	-0.9	1.0	-0.0	0.8	97
21176	03/11/92	42	3.9	3.0	-0.0	1.2	79	0.8	1.8	0.1	1.0	90
21190	04/11/92	36	3.2	1.6	0.0	1.0	83	0.9	1.3	-0.0	0.9	94
21303	12/11/92	37	2.8	1.7	0.1	1.0	81	1.8	1.5	-0.0	1.2	81
21557	30/11/92	26	2.6	1.1	-0.0	0.9	88	-0.9	1.1	-0.0	0.9	88
21769	15/12/92	25	3.7	2.5	0.0	1.1	80	-4.7	0.9	-0.0	0.8	92
25116	09/08/93	63	5.3	2.1	0.0	1.4	73	3.3	1.8	-0.1	1.2	78
25300	22/08/93	46	4.1	1.2	0.0	1.2	78	12.4	1.2	0.0	0.9	93
25314	23/08/93	68	4.2	2.0	0.0	1.2	78	11.0	1.6	-0.1	1.0	88
25342	25/08/93	51	3.0	1.4	0.1	1.3	82	8.9	1.9	-0.1	0.8	94
25399	29/08/93	49	5.2	3.0	-0.4	2.5	45	13.1	1.6	0.0	0.8	90
25780	25/09/93	37	3.8	1.2	-0.1	1.0	84	-19.3	0.7	0.0	0.7	91
26726	01/12/93	22	5.5	1.5	0.0	0.9	91	-7.3	1.6	-0.1	1.2	82

pts — no. of geographic features identified and analysed
$\overline{xt}$ — mean value of errors cross-track (linear pixels = 0.803 km)
σ_{xt} — standard deviation of errors cross-track (linear pixels)
$\overline{at}$ — mean value of errors along-track (lines = 1.1km)
σ_{at} — standard deviation of errors along-track (lines)
xt% — percent of identified chips with cross-track residual errors in range -1.5 to +1.5 linear pixels
at% — percent of identified chips with along-track residual errors in range -1.5 to +1.5 lines

Table 3: Summary of results for NOAA-11 afternoon (ascending) overpasses.

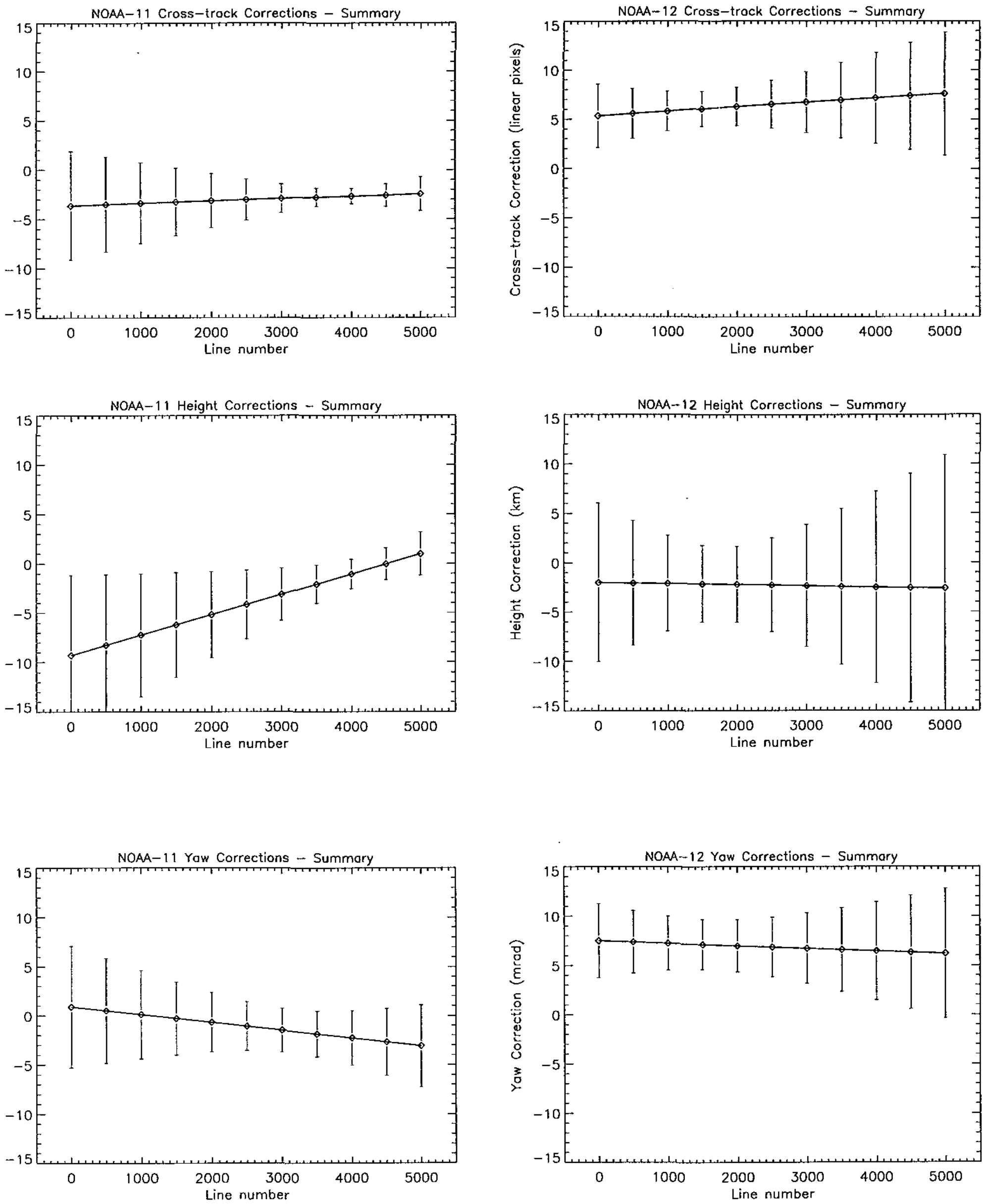

Figure 2: Plots showing summary of corrections applied to satellite position *vs* image line number.

orbit	date	pts	cross-track					along-track				
			pre-analysis		post-analysis			pre-analysis		post-analysis		
			$\overline{xt}$	σ_{xt}	$\overline{xt}$	σ_{xt}	$xt\%$	$\overline{at}$	σ_{at}	$\overline{at}$	σ_{at}	$at\%$
02021	03/10/91	15	-8.2	2.4	0.1	1.6	80	4.1	4.7	0.0	0.7	93
02106	09/10/91	25	-6.8	2.0	0.0	1.3	76	10.4	1.9	-0.0	0.7	100
02859	01/12/91	12	-7.5	2.6	0.3	1.8	42	4.4	3.1	0.1	0.6	100
03527	17/01/92	46	-6.1	1.2	0.0	1.0	83	-0.5	2.1	-0.0	0.9	93
03541	18/01/92	46	-7.6	1.0	0.1	1.0	92	5.9	1.9	0.0	0.7	100
03882	11/02/92	19	-9.5	2.4	-0.2	1.3	68	7.3	0.7	-0.1	0.7	95
06881	09/09/92	14	-6.9	1.6	0.0	0.6	100	2.2	1.5	0.0	0.7	100
06909	11/09/92	18	-5.9	2.2	-0.0	0.8	94	3.7	3.0	-0.1	1.0	83
06923	12/09/92	21	-6.3	2.4	0.0	1.0	81	4.9	2.0	0.0	0.8	90
06980	16/09/92	25	-6.4	2.0	0.0	1.0	92	9.7	2.8	0.0	0.8	96
07037	20/09/92	21	-6.3	1.4	0.1	1.2	71	0.9	1.2	0.1	0.7	100
08160	08/12/92	44	-7.7	1.9	0.2	1.4	73	8.7	3.0	-0.0	1.0	86
08757	19/01/93	29	-7.0	1.3	-0.0	1.1	86	8.4	1.2	-0.1	0.9	86
09866	07/04/93	17	-7.5	2.8	-0.0	1.0	82	0.8	3.2	0.0	0.7	100
11799	21/08/93	41	-5.5	1.5	0.1	1.2	83	10.8	2.0	0.0	0.9	90
11813	22/08/93	39	-9.6	2.2	0.1	1.6	62	16.3	2.8	0.1	0.9	90
11870	26/08/93	21	-5.5	1.6	0.1	1.4	71	17.7	1.9	0.0	0.9	95
12069	09/09/93	22	-8.3	2.6	-0.1	1.3	73	11.0	2.7	-0.0	1.0	82
12083	10/09/93	16	-6.7	1.8	-0.0	1.0	81	8.6	3.5	0.0	0.7	94
12097	11/09/93	11	-5.4	1.4	0.0	1.0	91	10.9	1.6	-0.0	0.9	91
12140	14/09/93	25	-9.2	2.1	-.0.	1.4	76	11.7	2.4	-0.0	0.8	96
12154	15/09/93	21	-7.5	2.6	-0.0	1.3	71	11.7	2.8	-0.0	0.7	100
12168	16/09/93	18	-9.5	4.4	-0.0	1.2	72	9.3	2.4	0.1	0.6	100
12183	17/09/93	15	-6.6	1.6	0.0	0.6	100	11.8	2.4	-0.0	1.0	87
12225	20/09/93	20	-7.6	4.0	-0.2	1.5	60	13.2	2.5	-0.2	0.9	85
12254	22/09/93	42	-5.0	1.3	-0.2	1.2	76	7.2	2.3	-0.1	0.9	88
12268	23/09/93	39	-6.0	1.5	0.0	1.0	87	12.0	2.0	-0.0	0.8	92
12282	24/09/93	40	-8.4	2.3	0.1	1.4	70	-8.8	4.5	-0.0	0.8	93
12296	25/09/93	16	-6.1	2.8	-0.0	1.1	81	-7.6	2.5	0.0	0.6	100
12438	05/10/93	20	-8.0	2.2	0.1	1.1	85	-4.9	1.6	0.0	0.6	100
12439	05/10/93	21	-7.0	1.4	-0.0	1.2	76	-3.5	3.0	-0.0	1.1	86
12453	06/10/93	50	-6.5	1.7	0.1	1.2	80	-3.5	2.1	0.1	0.9	88
12481	08/10/93	22	-7.0	1.8	-0.2	1.3	73	3.2	3.2	0.1	0.6	91
13220	29/11/93	17	-6.4	2.9	-0.0	1.2	82	0.0	3.1	-0.0	1.0	88
13320	06/12/93	28	-5.6	1.4	-0.0	1.1	86	-2.5	1.5	-0.0	0.8	89

Table 4: As for table 3 but for NOAA-12 morning (descending) overpasses.

Figure 2 does in fact show the expected bias in cross-track position correction for both the NOAA-11 and NOAA-12 satellites. The mean cross-track biases over land areas of -2.8 and 6.0 linear pixels for NOAA-11 and NOAA-12 respectively confirm the earlier reported values of -3.5 linear pixels (in the present terminology and sign convention) for NOAA-11 (Marsouin and Brunel, 1991) and 6.4 linear pixels for NOAA-12 (Brunel and Marsouin, 1992).

Figure 2 also reveals a small, persistent, negative bias in height correction over land for the NOAA-11 satellite and a persistent, positive bias in yaw correction of mean value $\sim$7.1 mrad for the NOAA-12 satellite. Brunel and Marsouin (1992) report navigation errors in AVHRR data which increase with increasing cross-track position. Their reported error gradient of .0058 line/pixel translates to a positive yaw correction of 7.1 mrad.

The observed cross-track and yaw biases suggest either the existence of an alignment

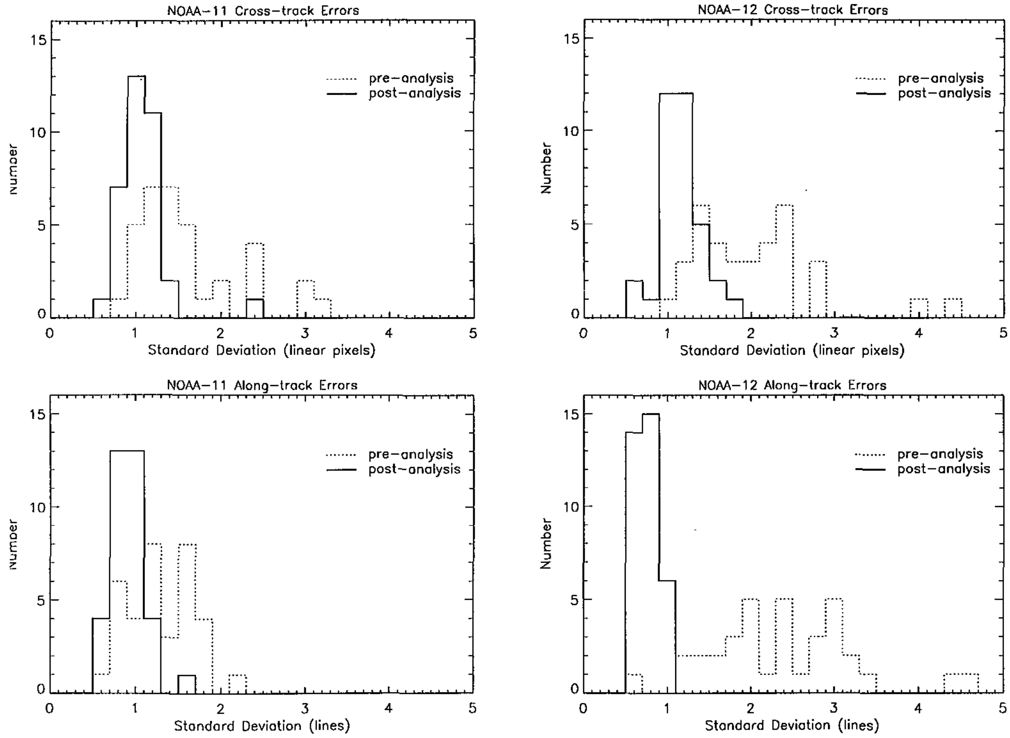

Figure 3: Plots showing histograms of standard deviation of errors pre- and post-analysis.

error in the AVHRR instrument relative to the spacecraft or an off-axis bias in the respective attitude control systems or both.

Examination of pre- and post-analysis values of mean cross-track and along-track errors listed in tables 3 and 4 shows that analysis has reduced the mean errors in every instance and generally from several pixels or lines to (usually small) fractions of a pixel or line.

Examination of pre- and post-analysis values for the standard deviation of errors listed in the tables shows a generally substantial reduction in variance following analysis. For NOAA-11 , the standard deviations of cross-track and along-track errors are reduced by an average 27% and 25% respectively. For NOAA-12 , the corresponding reductions are 38% and 61% respectively. The reduction in the variance of errors is shown graphically in the histograms of figure 3. For both satellites, pre-analysis values of standard deviations of cross-track errors collapse after analysis to a tight distribution about a value slightly in excess of 1.0 linear pixels. Similarly, standard deviations of along-track errors collapse to an even tighter distribution about a value slightly less than 1.0 lines. Geographically, the residual cross-track and along-track standard deviations are quite comparable and approximately equal to 1.0 km (1 linear pixel corresponds to 0.80 km amd 1 line corresponds to 1.1 km). This figure of 1.0

km represents a limit to accuracy which is related primarily to the accuracy of the underlying chip data set.

The tables also show the percentage of identified GCPs with cross-track and along-track residual errors that lie within the range ±1.5 linear pixels and ±1.5 lines respectively. The high values provide additional evidence of the general efficacy of the approach.

4.2 Operational Performance

Ultimately, the approach described here relies on the identification of land features to provide GCPs. Operationally, GCPs may not be identified in sufficient numbers or distribution to allow a full analysis of the type described above. For instance, an overpass may not include sufficiently large areas of land or the land that is included may be fully or partially obscured by cloud. Here we attempt to demonstrate the value of the approach as an operational procedure. To do so, we have catalogued in tables 5 and 6 the performance statistics as listed in SATLOC's report files for all overpasses covering land acquired by the DAR reception facility over a representative 33 day period commencing 30th August 1992.

Of the 44 NOAA-11 overpasses listed in table 5, 33 provide more than the 10 GCPs required for full analysis and give results similar to the full analysis examples discussed in the preceding section. (In point of fact, 5 of these 32 give no reduction with analysis of the variance of the errors. However, the initial standard deviation in these 5 cases is low and reduction from this low base would not be expected.) Analysis of the remaining 10 overpasses produced residual errors with a mean of fractions of a pixel or line. Variances were not reduced.

Of the 31 NOAA-12 overpasses listed in table 6, 19 provide sufficient GCPs for full analysis and give results consistent with the examples of full analysis already provided. Analysis of the remaining 12 again produced residual errors with a negligible mean value but no reduction in variance.

Tables 5 and 6 also show the percentage of identified GCPs with cross-track and along-track residual errors that lie within the range ±1.5 linear pixels and ±1.5 lines respectively. In only 3 of the 75 examples listed in these tables does this percentage figure for either cross-track or along-track residual errors fall below 50%.

5 Enhancements

As the table data indicate and usage has confirmed, the operational performance of the present approach is adequate for most purposes. However, experience gained in using the package suggests a number of possibly useful means of further refining the method and/or adapting it to meet specific requirements.

Obviously, the key to successful application of the method is the accurate identification of GCPs in sufficient numbers and with sufficicient distribution within the area of interest to allow accurate determination of satellite correction parameters. The number of GCPs identified could be increased if the number and distribution of chips were increased. The benefits of this action would be substantial, especially in cases where land areas are partially obscured by cloud. The number of chips used in the approach described here was limited by consideration of the resources required to create them.

orbit	date	pts	cross-track					along-track				
			pre-analysis		post-analysis			pre-analysis		post-analysis		
			$\overline{xt}$	σ_{xt}	$\overline{xt}$	σ_{xt}	$xt\%$	$\overline{at}$	σ_{at}	$\overline{at}$	σ_{at}	$at\%$
20258	30/08/92	37	2.5	1.3	-0.0	1.2	78	-2.8	1.5	0.0	1.1	78
20259	30/08/92	8	3.0	1.1	-0.0	1.1	88	-2.1	1.0	0.0	1.0	88
20272	31/08/92	33	2.3	1.0	0.0	0.9	88	2.0	1.2	-0.0	1.0	91
20273	31/08/92	4	5.5	1.8	0.0	1.8	50	-2.4	1.5	0.0	1.5	75
20286	01/09/92	7	2.9	1.0	0.1	1.0	86	1.9	0.6	0.8	0.6	86
20287	01/09/92	8	3.4	0.9	-0.3	0.9	100	0.6	0.6	0.6	0.6	100
20301	02/09/92	29	5.9	2.7	0.0	1.2	76	1.6	2.8	-0.0	0.7	100
20314	03/09/92	3	2.9	0.3	0.0	0.3	100	4.8	1.1	0.0	1.1	100
20315	03/09/92	20	5.5	2.2	-0.1	1.5	65	0.3	1.6	-0.1	1.2	90
20357	06/09/92	37	5.4	2.4	-0.0	1.2	70	-2.1	1.3	-0.1	0.8	95
20358	06/09/92	17	1.7	0.9	-0.0	0.9	88	-1.3	0.8	0.0	0.8	100
20371	07/09/92	38	4.1	1.3	0.0	1.1	79	-0.9	1.3	-0.0	1.0	87
20372	07/09/92	23	3.0	1.0	0.0	1.0	91	0.5	1.1	-0.0	1.0	87
20385	08/09/92	29	2.8	1.1	0.0	0.9	90	3.3	1.8	0.0	0.9	93
20386	08/09/92	4	7.7	1.6	0.8	1.6	75	-0.7	0.9	-0.8	0.9	75
20399	09/09/92	8	2.8	0.9	0.9	0.9	75	4.4	0.7	0.1	0.7	100
20400	09/09/92	24	4.2	3.4	0.0	1.3	83	2.3	2.1	0.0	0.8	96
20413	10/09/92	14	3.0	1.5	0.0	0.6	100	2.0	0.8	0.0	0.7	100
20414	10/09/92	35	4.1	1.6	0.0	1.0	77	6.4	2.3	-0.0	0.8	94
20427	11/09/92	10	2.1	1.3	0.4	1.3	70	2.4	1.1	-0.2	1.1	90
20428	11/09/92	6	4.9	1.4	0.7	1.4	75	-3.3	1.2	0.2	1.1	75
20442	12/09/92	18	3.8	1.6	-0.0	1.0	51	-7.2	5.6	0.0	1.2	78
20456	13/09/92	53	3.4	1.8	0.1	1.2	77	1.9	1.7	0.0	1.1	79
20470	14/09/92	36	4.7	2.7	-0.1	1.4	67	0.8	2.0	0.0	1.1	83
20484	15/09/92	13	2.8	1.6	-0.0	1.3	85	0.8	1.6	0.0	1.2	85
20498	16/09/92	47	2.5	1.3	-0.0	1.0	89	0.8	1.6	-0.0	0.8	96
20512	17/09/92	36	2.4	1.1	-0.0	1.0	92	0.6	1.2	-0.0	1.0	86
20513	17/09/92	6	3.7	1.8	0.0	1.8	50	-0.4	1.0	0.0	1.0	100
20526	18/09/92	28	2.8	1.1	0.0	1.0	86	4.8	0.9	0.0	0.9	86
20527	18/09/92	27	4.6	2.6	0.0	1.0	85	3.6	2.4	0.0	0.7	100
20540	19/09/92	19	2.7	1.0	0.1	1.0	84	2.1	0.7	0.1	0.7	100
20541	19/09/92	22	4.2	1.7	-0.0	1.1	86	0.1	1.9	-0.0	0.6	100
20555	20/09/92	22	4.6	2.7	0.1	1.0	91	3.8	1.6	0.0	1.1	86
20569	21/09/92	19	3.3	1.0	-0.0	0.9	95	2.2	1.7	-0.0	1.5	68
20583	22/09/92	17	3.2	1.7	0.0	0.9	88	3.1	1.6	0.0	1.2	71
20597	23/09/92	48	3.9	2.4	-0.0	1.1	88	4.5	1.9	-0.0	0.9	90
20598	23/09/92	15	2.5	0.8	-0.0	0.8	93	5.4	0.9	0.0	0.9	93
20639	26/09/92	33	1.7	1.3	-0.0	1.0	79	2.2	0.9	-0.0	0.8	94
20640	26/09/92	17	2.0	1.4	0.0	0.7	88	1.1	1.5	0.0	0.7	100
20667	28/09/92	8	2.0	1.4	-0.0	1.4	75	2.9	0.6	-0.0	0.6	100
20668	28/09/92	12	4.2	2.0	-0.1	0.8	100	-2.4	1.4	-0.1	1.4	75
20682	29/09/92	23	2.5	1.5	-0.0	0.8	96	0.0	1.9	-0.0	1.1	78
20696	30/09/92	25	5.1	3.3	0.1	1.6	72	4.6	1.7	-0.1	1.2	80
20711	01/10/92	15	1.6	1.2	0.0	1.2	73	1.7	0.8	-0.0	0.8	93

Table 5: As for table 3 but for NOAA-11 afternoon (ascending) overpasses for a 33 day period commencing 30th August 1992.

orbit	date	pts	cross-track					along-track				
			pre-analysis		post-analysis			pre-analysis		post-analysis		
			$\overline{xt}$	σ_{xt}	$\overline{xt}$	σ_{xt}	$xt\%$	$\overline{at}$	σ_{at}	$\overline{at}$	σ_{at}	$at\%$
06738	30/08/92	8	-8.8	1.2	0.0	1.2	88	4.6	0.7	0.0	0.7	100
06739	30/08/92	5	-5.7	1.6	0.0	1.6	60	3.5	1.6	0.0	1.6	60
06753	31/08/92	5	-6.7	1.2	0.0	1.2	80	0.2	0.9	0.0	0.9	100
06767	01/09/92	14	-7.5	1.8	0.1	1.5	79	1.8	2.8	-0.1	0.6	100
06781	02/09/92	6	-7.8	0.6	0.1	0.6	100	3.3	0.6	-0.0	0.6	100
06795	03/09/92	15	-6.5	1.2	0.1	1.2	87	3.6	1.0	0.0	0.9	87
06838	06/09/92	9	-6.1	1.2	-0.0	1.2	78	5.2	0.6	0.0	0.6	100
06852	07/09/92	6	-6.9	2.1	-0.3	2.1	17	9.2	1.3	0.1	1.3	83
06866	08/09/92	4	-7.7	1.0	0.0	1.0	100	5.9	0.6	0.0	0.6	100
06867	08/09/92	15	-7.2	2.1	0.1	1.4	67	7.1	3.4	0.1	1.2	73
06881	09/09/92	14	-6.9	1.6	0.0	0.6	100	2.2	1.5	0.0	0.7	100
06895	10/09/92	12	-8.9	1.4	0.0	0.8	100	8.6	3.8	0.0	0.6	100
06909	11/09/92	18	-5.9	2.2	-0.0	0.8	94	3.7	3.0	-0.1	1.0	83
06923	12/09/92	21	-6.3	2.4	0.0	1.0	81	4.9	2.0	0.0	0.8	90
06937	13/09/92	21	-9.2	1.7	0.1	1.7	67	7.7	0.9	0.0	0.8	90
06938	13/09/92	12	-6.8	3.0	-0.1	1.2	83	7.3	3.3	0.1	1.1	83
06952	14/09/92	5	-5.4	1.3	0.0	1.3	80	8.1	1.2	0.0	1.2	80
06980	16/09/92	25	-6.4	2.0	0.0	1.0	92	9.7	2.8	0.0	0.8	96
06994	17/09/92	17	-7.1	2.2	0.1	1.0	88	-0.4	1.9	-0.0	0.8	100
06995	17/09/92	6	-7.2	1.2	-0.0	1.2	83	-3.7	1.9	-0.0	1.9	67
07008	18/09/92	10	-10.8	1.6	-0.0	1.6	40	8.7	0.8	-0.0	0.7	100
07009	18/09/92	22	-5.6	1.3	0.1	1.1	86	4.1	1.4	-0.0	1.1	73
07023	19/09/92	39	-7.1	1.6	0.1	1.6	64	3.9	2.3	-0.0	0.8	85
07037	20/09/92	21	-6.3	1.4	0.1	1.2	71	0.9	1.2	0.1	0.7	100
07065	22/09/92	5	-6.3	1.6	0.0	1.6	80	5.9	0.6	0.0	0.6	100
07066	22/09/92	5	-5.8	0.7	0.0	0.7	100	6.1	2.1	0.0	2.1	40
07108	25/09/92	25	-6.6	2.0	0.0	1.4	64	9.4	3.0	0.0	0.8	96
07122	26/09/92	14	-7.0	1.2	-0.0	1.4	64	-6.3	1.8	0.0	0.8	93
07151	28/09/92	11	-6.8	1.7	0.1	0.7	100	7.5	1.9	0.0	1.0	91
07165	29/09/92	19	-9.6	2.7	-0.1	1.3	53	6.5	3.3	-0.0	0.8	95
07193	01/10/92	13	-12.0	3.5	-0.1	1.1	77	0.9	2.5	-0.1	1.0	85

Table 6: As for table 5 but for NOAA-12 morning (descending) overpasses.

The distribution of chips is necessarily uneven when working with the Australian land mass; whereas coastal areas provide abundant opportunities for chip creation, the vast inland areas are typically devoid of appropriate features. The chip set used in the work reported here included the confluence of rivers, distinctive meanderings of water courses and coves and peninsulas in inland lakes. While more chips covering these features could have been created had resources allowed, the significant bias towards chips of coastal areas would not have been redressed. The problem is less pronounced in other areas. For example, a chip library was made for the region immediately to the North of Australia. The large number of islands spread throughout that area allowed a chip library to be created with a relatively uniform geographical distribution.

Another difficulty sometimes arises with chips of inland features: frequently, a substantial fraction of the area covered by an inland chip is vegetated land and both the vegetation and its spectral signal are subject to seasonal change. The pattern of vegetation sometimes changes sufficiently to cause the correlation between an image feature and its corresponding chip to fall below the specified critical value and the feature remains unidentified. To some extent this problem could be solved by creating seasonally specific chips for the same feature and arranging for the chip appropriate to a particular image to to be selected. Such measures require significant additional effort and were not implemented here.

Very occasionally the correlation method used here falsely locates a chip's central feature at some distance from the corresponding real feature in the image. Almost always this behaviour is due to the presence in the image of cloud which in some way mimics the characteristics of the feature — for example, a cloud which has the shape of an underlying coastline but which is displaced a small distance from it. One way of avoiding this sort of error is to pass the image first through a cloud detection algorithm and then use only cloud-free data in the correlation procedure. In the absence of a failsafe cloud detection algorithm this solution is not employed here. Instead, points with excessive residual errors are assumed to be falsely located and eliminated in the course of processing. The cloud detection approach is more direct and its incorporation in any future implementation is recommended.

The performance analysis presented above suggests that the accuracy of the method may have reached a fundamental limit imposed by the accuracy of the underlying chip data set — which, of course, has a resolution of 1 pixel. Others, notably Cracknell and Paithoonwattanakij (1989) and Robertson *et al.* (1992), have addressed this issue by constructing chips from Landsat MSS data and have reported navigation accuracies of less than one pixel.

The present method has been modified for application to nighttime images (P. J. Turner, private communication). Chip sets are created using all 5 bands and hence require no modification. SATLOC was changed to perform correlations using band 4 data (a thermal band with a wavelength centred at 11 μm) instead of the band 2 data used for daytime images and the criteria for identification of a GCP was changed to $|r_0| > 0.80$ (*cf.* here, $r_0 > 0.90$). The fact that a nighttime image of a feature may be the negative of a chip created from a daytime image forced the need to include high negative correlations in the criteria for identification of a GCP. In addition, a rudimentary cloud detection algorithm was applied to the image data and only cloud-free data were used in the correlation procedure. No detailed analysis of the performance of the nighttime algorithm has been made but analysis of early results showed a satisfactory level of performance.

6 Conclusion

The navigation of AVHRR data using automatic land feature location in the imagery to fine tune model predictions of satellite position and attitude gives more accurate results than can be obtained using model predictions alone. When the number and distribution of land features located in an image are sufficient for full analysis, the method described here provides navigation to an accuracy of $\sim \pm 1$ pixel/line over the central 1600 pixels of the full image. Operational experience shows that such performance is achieved for ($\sim$ 60-70% of daytime overpasses. Performance degrades with failure to locate sufficient land features for full analysis but even in the worst case scenario where only one or two features are located, corrections are applied to satellite cross-track and along-track position so that the mean navigational error is reduced to a small fraction of a pixel/line while the standard deviation of the error remains at its pre-analysis level.

Some corrections to the model of satellite position and attitude show a persistent bias. The mean cross-track correction for the NOAA-11 satellite is −2.4 linear pixels while that for the NOAA-12 satellite is 6.0 linear pixels. The mean yaw correction for NOAA-12 is 7.1 mrad. These figures support earlier published data.

7 Acknowledgements

We wish to acknowledge the very significant contributions made to this work by Janice Bathols and Mary Edwards of DAR. They developed techniques and skills in the creation of effective chips and built libraries of these covering the Australian continent for both ascending and descending overpasses. Their constructive comments and suggestions influenced the development of the method reported here.

We also thank Steve Clift of CSIRO, Division of Oceanography, who supplied code for the Brouwer-Lyddane satellite orbital model employed here. The latter proved more stable than the Brouwer model used at DAR.

References

Baldwin, D. G. and Emery, W. J. (1993): A systematized approach to AVHRR image navigation, *Annals of Glaciology*, **17**, 414–420.

Bordes, P., Brunel, P. and Marsouin, A. (1992): Automatic adjustment of AVHRR navigation, *J. of Atmospheric and Oceanic Technology*, **9**, 15–27.

Brouwer, D. (1959): Solution of the problem of artificial satellite theory with drag, *The Astronomical J.*, **64**, 378–397.

Brouwer, D. and Clemence, G. M. (1961): *Methods of Celestial Mechanics.* Academic Press, New York. 568pp.

Brunel, D. and Marsouin, A. (1989): Navigation of AVHRR images using ARGOS or TBUS orbital elements. *Proc. 4th AVHRR Data Users' Meeting*, Rothenburg, F. R. Germany, 5-8 September 1989, EUM06, 11–15.

Brunel, D. and Marsouin, A. (1992): Systematic navigation error on NOAA-12 AVHRR images, *Int. J. of Remote Sensing*, 14, 171–176.

Cappellari, J. O., Velez, C. E. and Fuchs, A. J. (1976): *Mathematical Theory of the Goddard Trajectory Determination System.* Technical Report X-582-76-77, Goddard Space Flight Center, Greenbelt, MD, USA. 599pp.

Cracknell, A. and Paithoonwattanakij, K. (1989): Pixel and sub-pixel accuracy in geometrical correction of AVHRR imagery, *J. of Remote Sensing*, **10**, 661–667.

Eidenshink, J. C. (The 1990 conterminous U. S. AVHRR data set): 1992, *Photogrammetric Engineering and Remote Sensing*, **58**, 809–813.

Emery, W. J., Brown, J. and Nowak, Z. P. (1989): AVHRR Image Navigation: Summary and Review, *Photogrammetric Engineering and Remote Sensing*, **55**, 1175–1183.

Jullien, J. P. and Phulpin, T. (1988): Ajustement automatique de la navigation AVHRR. Note de Travail de l'EERM, METEOFRANCE. 1–30.

Kloster, K. (1989): Using TBUS orbital elements for AVHRR image gridding, *Int. J. of Remote Sensing*, **10**, 653–659.

Krasnopolsky, V. M. and Breaker, L. C. (1994): The problem of AVHRR image navigation revisted, *Int. J. of Remote Sensing*, **15**, 979–1008.

Lyddane, R. H. (1963): Small eccentricities or inclinations in the Brouwer theory of the artificial satellite, *The Astronomical J.*, **68**, 555–558.

Marsouin, A. and Brunel, D. (1991): Navigation of AVHRR images using ARGOS or TBUS bulletins, *Int. J. of Remote Sensing*, **12**, 1575–1592.

Planet, W. G. (1988): *Data Extraction and Calibration of TIROS-N/NOAA Radiometers.* NOAA Technical Memorandum NESS 107 — Rev 1, National Technical Information Service (NTIS), U. S. Department of Commerce, Sills Bldg., 5285 Port Royal Road, Springfield, VA 22161, USA. 57pp, Appendices.

Robertson, B., Erickson, A., Friedel, J., Guindon, B., Fisher, T., Brown, R., Teillet, P., D'Iorio, M., Cihlar, J. and Sanz, A. (1992): GEOCOMP, a NOAA AVHRR data geocoding and compositing system. In:*Proceedings of ISPRS Washington '92, International Archives of Photogrammetry and Remote Sensing*, Vol. XXIX Part B2, Commission II, pp 223-228.

Schwalb, A. (1982): *Modified Version of the Tiros N/NOAA A-G Satellite Series (NOAA E–J) — Advanced TIROS N (ATN).* NOAA Technical Memorandum NESS 116, edited by National Technical Information Service (NTIS), U. S. Department of Commerce, Sills Bldg., 5285 Port Royal Road, Springfield, VA 22161, USA. 23pp.

Torlegård, A. K. I. (1986): Some photogrammetric experiments with digital image processing, *Photogrammetric Record*, **12**, 175–186.

Wright, S. J. and Holt, J. N. (1985): Algorithms for non-linear least squares with linear inequality constraints, *SIAM J. Sci. Stat. Comput.* , **6**, 1033–1048.

CSIRO DIVISION OF ATMOSPHERIC RESEARCH TECHNICAL PAPERS

No. 1 Galbally, I. E.; Roy, C. R.; O'Brien, R. S.; Ridley, B. A.; Hastie, D. R.; Evans, W. J. F.; McElroy, C. T.; Kerr, J. B.; Hyson, P.; Knight, W.; Laby, J. E.
Measurements of trace composition of the Austal stratosphere: chemical and meteorological data. 1983. 31 p.

No. 2 Enting, I. G.
Error analysis for parameter estimates from constrained inversion. 1983. 18 p.

No. 3 Enting, I. G.; Pearman, G. I.
Refinements to a one-dimensional carbon cycle model. 1983. 35 p.

No. 4 Francey, R. J.; Barbetti, M.; Bird, T.; Beardsmore, D.; Coupland, W.; Dolezal, J. E.; Farquhar, G. D.; Flynn, R. G.; Fraser, P. J.; Gifford, R. M.; Goodman, H. S.; Kunda, B.; McPhail, S.; Nanson, G.; Pearman, G. I.; Richards, N. G.; Sharkey, T. D.; Temple, R. B.; Weir, B.
Isotopes in tree rings. 1984. 86 p.

No. 5 Enting, I. G.
Techniques for determining surface sources from surface observations of atmospheric constituents. 1984. 30 p.

No. 6 Beardsmore, D. J.; Pearman, G. I.; O'Brien, R. C.
The CSIRO (Australia) Atmospheric Carbon Dioxide Monitoring Program: surface data. 1984. 115 p.

No. 7 Scott, John C.
High speed magnetic tape interface for a microcomputer. 1984. 17 p.

No. 8 Galbally, I. E.; Roy, C. R.; Elsworth, C. M.; Rabich, H. A. H.
The measurement of nitrogen oxide (NO, NO_2) exchange over plant/soil surfaces. 1985. 23 p.

No. 9 Enting, I. G.
A strategy for calibrating atmospheric transport models. 1985. 25 p.

No. 10 O'Brien, D. M.
TOVPIX: software for extraction and calibration of TOVS data from the high resolution picture transmission from TIROS-N satellites. 1985. 41 p.

No. 11 Enting, I. G.; Mansbridge, J. V.
Description of a two-dimensional atmospheric transport model. 1986. 22 p.

No. 12 Everett, J. R.; O'Brien, D. M.; Davis, T. J.
A report on experiments to measure average fibre diameters by optical fourier analysis. 1986. 22 p.

No. 13 Enting, I. G.
A signal processing approach to analysing background atmospheric constituent data. 1986. 21 p.

No. 14 Enting, I. G.; Mansbridge, J. V.
Preliminary studies with a two- dimensional model using transport fields derived from a GCM. 1987. 47 p.

No. 15 O'Brien, D. M.; Mitchell, R. M.
Technical assessmant of the joint CSIRO/Bureau of Meteorology proposal for a geostationary imager/ sounder over the Australian region. 1987. 53 p.

No. 16 Galbally, I. E.; Manins, P. C.; Ripari, L.; Bateup, R.
A numerical model of the late (ascending) stage of a nuclear fireball. 1987. 89 p.

No. 17 Durre, A. M.; Beer, T.
Wind information prediction study: Annaburroo meteorological data analysis. 1989. 30 p. + diskette.

No. 18 Mansbridge, J. V.; Enting, I. G.
Sensitivity studies in a two- dimensional atmospheric transport model. 1989. 33 p.

No. 19 O'Brien, D. M.; Mitchell, R. M.
Zones of feasibility for retrieval of surface pressure from observations of absorption in the A band of oxygen. 1989. 12 p.

No. 20 Evans, J. L.
Envisaged impacts of enhanced greenhouse warming on tropical cyclones in the Australian region. 1990. 31 p. [Out of print]

No. 21 Whetton, P. H.; Pittock, A. B.
Australian region intercomparison of the results of some general circulation models used in enhanced greenhouse experiments. 1991. 73 p. [Out of print]

No. 22 Enting, I. G.
Calculating future atmospheric CO_2 concentrations. 1991. 32 p.

No. 23 Kowalczyk, E. A.; Garratt, J. R.; Krummel, P. B.
A soil-canopy scheme for use in a numerical model of the atmosphere — 1D stand-alone model. 1992. 56 p.

No. 24 Physick, W. L.; Noonan, J.A.; McGregor, J.L.; Hurley, P.J.; Abbs, D.J.; Manins, P.C.
LADM: A Lagrangian Atmospheric Dispersion Model. 1994. 137 p.

No. 25 Enting, I. G.
Constraining the atmospheric carbon budget: a preliminary assessment. 1992. 28 p.

No. 26 McGregor, J. L.; Gordon, H. B.; Watterson, I. G.; Dix, M. R.; Rotstayn, L. D.
The CSIRO 9-level atmospheric general circulation model. 1993. 89 p.

No. 27 Enting, I. G.; Lassey, K. R.
Projections of future CO_2. with appendix by R. A. Houghton. 1993. 42 p.

No. 28 [Not published]

No. 29 Enting, I. G.; Trudinger, C. M.; Francey, R. J.; Granek, H.
Synthesis inversion of atmospheric CO_2 using the GISS tracer transport model. 1993. 44 p.

No. 30 O'Brien, D. M.
Radiation fluxes and cloud amounts predicted by the CSIRO nine level GCM and observed by ERBE and ISCCP. 1993. 37 p.

No. 32 Kowalczyk, E.A.; Garratt, J.R.; Krummel, P.B.
Implementation of a soil-canopy scheme into the CSIRO GCM — regional aspects of the model response. 1994.

No. 33 Prata, A.J.
Validation data for land surface temperature determination from satellites. 1994. 40 p.